

Article

Natural Clay Minerals as a Starting Material for Matrices for the Immobilization of Radioactive Waste from Pyrochemical Processing of SNF

Anna V. Matveenko¹, Andrey P. Varlakov², Alexander A. Zhrebtsov³, Alexander V. Germanov², Ivan V. Mikheev¹ , Stepan N. Kalmykov¹ and Vladimir G. Petrov^{1,*} 

¹ Department of Chemistry, Lomonosov Moscow State University, 119991 Moscow, Russia;

avd.msk11@mail.ru (A.V.M.); mikheev.ivan@gmail.com (I.V.M.); stepan@radio.chem.msu.ru (S.N.K.)

² JSC "A.A. Bochvar High-Technology Scientific Research Institute for Inorganic Materials (VNIINM)", 123098 Moscow, Russia; varlakov_a@mail.ru (A.P.V.); avgermanov@bochvar.ru (A.V.G.)

³ JSC "Proryv", 107140 Moscow, Russia; zhala@proryv2020.ru

* Correspondence: vladimir.g.petrov@gmail.com

Abstract: Pyrochemistry is a promising technology that can provide benefits for the safe reprocessing of relatively fresh spent nuclear fuel with a short storage time (3–5 years). The radioactive waste emanating from this process is an electrolyte (LiCl–KCl) mixture with fission products included. Such wastes are rarely immobilized through common matrices such as cement and glass. In this study, samples of ceramic materials, based on natural bentonite clay, were studied as matrices for radioactive waste in the form of LiCl–KCl eutectic. The phase composition of the samples, and their mechanical, hydrolytic, and radiation resistance were characterized. The possibility of using bentonite clay as a material for immobilizing high-level waste arising from pyrochemical processing of spent nuclear fuel is further discussed in this paper.

Keywords: pyrochemical process; radioactive waste; immobilization; bentonite; ceramic matrices; spent nuclear fuel



Citation: Matveenko, A.V.; Varlakov, A.P.; Zhrebtsov, A.A.; Germanov, A.V.; Mikheev, I.V.; Kalmykov, S.N.; Petrov, V.G. Natural Clay Minerals as a Starting Material for Matrices for the Immobilization of Radioactive Waste from Pyrochemical Processing of SNF. *Sustainability* **2021**, *13*, 10780. <https://doi.org/10.3390/su131910780>

Academic Editors: Changhyun Roh, Michael I. Ojovan, Vladislav A. Petrov and Sergey V. Yudintsev

Received: 9 August 2021

Accepted: 24 September 2021

Published: 28 September 2021

Publisher's Note: MDPI stays neutral with regard to jurisdictional claims in published maps and institutional affiliations.



Copyright: © 2021 by the authors. Licensee MDPI, Basel, Switzerland. This article is an open access article distributed under the terms and conditions of the Creative Commons Attribution (CC BY) license (<https://creativecommons.org/licenses/by/4.0/>).

1. Introduction

Countries that use nuclear energy, including Russia, have accumulated large volumes of radioactive waste (RW) of various activity levels and aggregate states. Their main source of radioactive waste comes from the processing of spent nuclear fuel (SNF) from energetic, transport (marine), and research reactors. Converting solid RW, including slags, into a chemically and mechanically stable form suitable for final disposal, in order to isolate RW from the biosphere, is an urgent scientific, technical, and social task, and a viable solution would significantly increase the level of radiation safety for the population.

Among all types of radioactive waste, high-level waste (HLW) is the most dangerous and is dominated by ⁹⁰Sr, ¹³⁷Cs and ⁶⁰Co radionuclides, whose total activity can amount to 95% of the total activity of stored radioactive waste. The generally accepted approach to solving the problem of HLW management is its conversion to a solid state (for liquid waste), its inclusion into strong phases (preserving matrices) and its further disposal in underground storage facilities. At present, vitrified materials are used to immobilize HLW on an industrial scale; borosilicate glasses are still the main form used for the immobilization of high-level radioactive wastes [1].

In view of the task to close the fuel cycle, the Breakthrough (Proryv) project in Russia was launched for the reprocessing of mixed uranium–plutonium nitride (MNUP) SNF using pyrochemical or combined technology (pyrochemistry + hydrometallurgy), where the use of molten salt LiCl–KCl is assumed [2]. In contrast to technological processes in aqueous–organic systems, processes in chloride melts have advantages such as high radiation resistance of the liquid phase, internal safety of the processes, the possibility

of regenerating spent nuclear fuel with a short exposure time, and a smaller amount of generated radioactive waste. However, the industrial application of pyrochemical processing technology cannot be carried out until the best methods for the disposal of the resulting radioactive wastes are determined. In this case, the LiCl–KCl eutectic with included fission products (FP) will act as the waste (Figure 1).

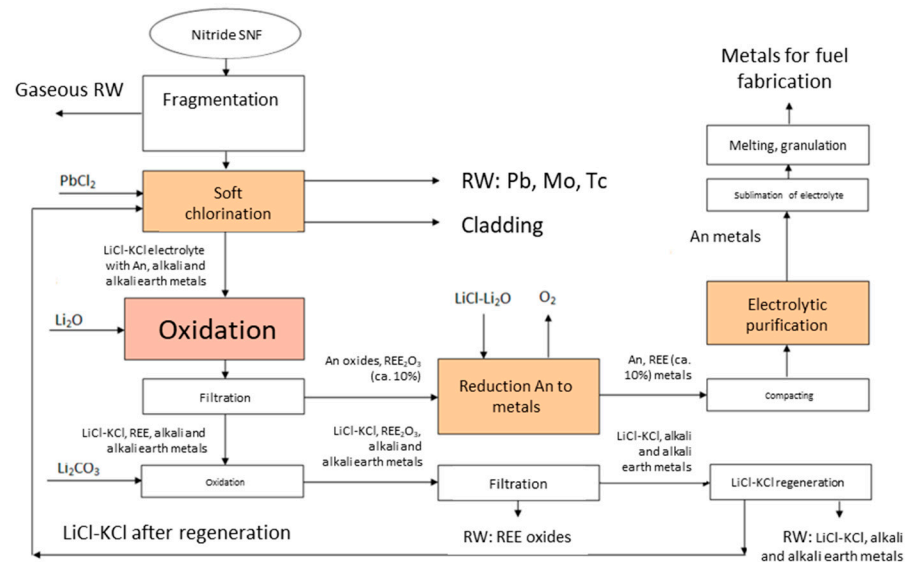


Figure 1. The technological optional scheme for pyrochemical processing of nitride SNF.

Chloride salts are difficult to immobilize in both glass matrices and cements, and in most types of ceramics. Studies of new glass compositions and glass-based composite materials show that the reliable fixation of significant amounts of alkali metals' chlorides requires preliminary treatment and their transformation to the form of oxides or phosphates, i.e., an additional technological operation is required [3–6].

In addition, the research results indicate an instability of glasses in groundwater, especially after their spontaneous devitrification (crystallization) during storage as an effect of ionizing radiation and chemical processes inside the glasses. The destruction of glass matrices due to crystallization will lead to a decrease in their chemical stability and, as a consequence, to the release of radionuclides, including long-lived ones, into the environment. Therefore, the development of alternative crystalline (mineral-like) matrices for the immobilization of high-level waste is an urgently required scientific task [7–9].

The main requirements to matrix materials are: a high isomorphic capacity for waste components (the ability to include a significant amount of waste in the bulk composition), high chemical and radiation stability (it is necessary to minimize the release of radionuclides during possible contact with groundwater), mechanical strength (it must not disintegrate during transportation, storage operations, etc.), as well as an easy industrial production process. The selection of suitable phases, with the listed properties, is conducted on the basis of the results of geochemical, mineralogical, and crystal–chemical studies of natural minerals and synthetic compounds.

Existing work on the properties of crystalline ceramics for immobilizing radioactive waste is related to mineral-like phases such as pyrochlore, perovskite, zirconolite, zirconium dioxide, garnet, hollandite, pollucite, murataite, monazite, and NZP [10–17]. The authors of [18] developed a method for immobilizing chloride salts using zeolite with sodalite as the final form of the transformed chlorides. This method involves a technologically complex and long-term process of zeolite occlusion to uniformly distribute alkali chlorides over zeolite cells. Chloride incorporation in such a material is negligible, which proves to be a problem for all chloride-containing matrices. Similar methods of incorporating salt waste (chlorides and iodides of alkali metals) into sodalite and zeolite matrices are described in [19–23].

In this work, we investigated the use of natural clay minerals as a possible matrix material for waste produced from pyrochemical processing of SNF in the form of LiCl–KCl eutectic that included fission products. The mineral-like materials will decrease the diffusion of radionuclides from the matrix into the biosphere because the matrix material, in its chemical and phase composition, will be similar to the host rocks of the waste repository.

2. Materials and Methods

The aim of this work was to develop a method for the anhydrous conversion of mono- and bivalent s-elements' chlorides into a stable, mineral-like structure. To achieve this, we used bentonite clays, that (a) are finely dispersed materials consisting of at least 70% of the layered mineral montmorillonite, (b) have a large specific surface area, (c) just as all clays, become very strong upon annealing, and (d) are able to retain their alkali metals due to their layered structure. This option may be the most promising in order to ensure the reliable long-term isolation of radionuclides from the environment.

In this study, we prepared samples of bentonite clay with a chloride mixture (CIM) content of at least 20 wt.%, of various compositions, as well as samples of bentonite clays with various silicon-containing additives and the inclusion of the at least 20 wt.% of the LiCl–KCl eutectic. The compositions of the main studied samples included the simulated spent electrolyte and are presented in Table 1. In addition to monovalent and bivalent elements, we also used analogs of trivalent and tetravalent f-elements, since such elements can contaminate the spent electrolyte.

Table 1. Composition of the samples studied in the work with different composition of the simulated spent chloride mixture and silicon-containing additives.

Sample Code	Composition of the Ceramic Base	Content, wt.%					
		LiCl	KCl	CsCl	SrCl ₂	CeCl ₃	ZrOCl ₂
B20-0	Bentonite + 20 wt.% LiCl–KCl eutectic	44	56	-	-	-	-
B20-1	Bentonite + 20 wt.% CIM1	40	50	10	-	-	-
B20-2	Bentonite + 20 wt.% CIM2	40	50	5	5	-	-
B20-3	Bentonite + 20 wt.% CIM3	40	50	3	3	4	-
B20-4	Bentonite + 20 wt.% CIM4	40	50	3	3	-	4
B + mcrSi3	Bentonite + 3 wt.% microcryst.silica + 20 wt.% CIM	44	56	-	-	-	-
B + mcrSi5	Bentonite + 5 wt.% microcryst.silica + 20 wt.% CIM	44	56	-	-	-	-
B + mcrSi10	Bentonite + 10 wt.% microcryst.silica + 20 wt.% CIM	44	56	-	-	-	-
B + NaSi3	Bentonite + 3 wt.% Na ₂ SiO ₃ + 20 wt.% CIM	44	56	-	-	-	-
B + NaSi5	Bentonite + 5 wt.% Na ₂ SiO ₃ + 20 wt.% CIM	44	56	-	-	-	-
B + NaSi10	Bentonite + 10 wt.% Na ₂ SiO ₃ + 20 wt.% CIM	44	56	-	-	-	-
B + A3	Bentonite + 3 wt.% AEROSIL + 20wt.% CIM	44	56	-	-	-	-
B + A5	Bentonite + 5 wt.% AEROSIL + 20wt.% CIM	44	56	-	-	-	-
B + A10	Bentonite + 10 wt.% AEROSIL + 20 wt.% CIM	44	56	-	-	-	-

The mixture of chlorides was ground, dehydrated in an oven at 250 °C for 2 h, and then stored in a desiccator over P₂O₅. Then, all the samples were prepared by mixing and grinding CIM with the main components of the matrices, after which the mixture was dried at 100–150 °C and pressed into tablets with a diameter of 10 mm and a height of 2–4 mm or 8–10 mm (for some tests) using a hand press. The last two stages of temperature preparation, the parameters of which were determined using some additional analyses, were carried out in a muffle furnace: the samples were dried at 400 °C for 4 h, ground again and pressed into tablets to obtain a more homogeneous product, and at the end they were annealed for 12 h at 900 °C (below the sintering temperature of pure bentonite).

Thermal characteristics of the prepared mixtures were investigated with a NETZSCH STA 449 C/4/G Jupiter device (Germany) with synchronous gas phase analysis using a NETZSCH 403C Aeolos quadrupole mass spectrometer (Germany). The analysis was carried out in the temperature range 40–1000 °C at a rate of 10 K/min.

The mechanical strength of each ceramic sample was determined by first measuring the maximum load that each sample could withstand without breaking, and then calculating the stresses at these given loads. A Cybertronic Cyber-Plus Evolution testing machine was used for such purposes. Three parallel samples were used for measurements; the average value calculated using the three measurements was taken as the result of the strength tests.

The phase composition of each of the samples and its change during the heating process was measured using an Empyrean, Panalytical X-ray powder diffractometer with a furnace and the ability to reach heats of up to 1200 °C (CuK_α radiation, two wavelengths were taken into account in the calculations: 1.5406 and 1.5444 Å with an intensity ratio in the doublet of 2:1). The phase composition of the samples was studied by heating them from room temperature to 1000 °C.

The chemical stability of the samples was studied according to the standard procedure, under static conditions, and at 25 °C in accordance with standard protocol GOST P 52126-2003. The pre-synthesized tablets were placed in plastic cups with a lid in 10 mL of distilled water. At specific time intervals, the solution was poured out, water samples were taken for chemical analysis, and a new portion of water was poured into the glass. An analysis of the leachates was performed using an ICP-AES and ionic chromatography.

The leaching rate was calculated using the following equations:

$$NL = \frac{a}{f \times S}; \quad (1)$$

$$R = \frac{NL}{t}, \quad (2)$$

where R is the leaching rate, g/(cm²·day);

NL is normalized weight loss, g/cm²;

t is the time interval, in days;

a is the mass of the element that has passed into the solution, g;

f is the mass fraction of the element in the sample;

S is the sample surface in cm².

To determine their radiation resistance, the ceramic samples were irradiated on an electron accelerator for a month, with a maximum dose of 10⁹ Gy, after which the surface morphology, phase composition, and mechanical characteristics of the samples were investigated.

3. Results and Discussion

3.1. Thermal Analysis

To determine the optimal time–temperature parameters for synthesis, we performed a thermogravimetric analysis and differential scanning calorimetry. The results of these are presented in Figure 2a. Water was released during the first stage, (200–250 °C), possibly due to the preservation of the primary layered structure of montmorillonite. During the second stage, the mineral began to lose water, represented in the hydroxyl groups of the layers, and at temperatures of 500–600 °C the mineral turned into an anhydrous modification; the transition of hydroxyl groups to oxol groups also occurred with the release of water.

Thus, the thermochemical binding of the components of pyrochemical waste reprocessing ended, and the metal cations present in the spent electrolyte were incorporated into the crystal structure. According to the analysis of off-gas mass spectrometry, at higher temperatures, weight loss was due to the release of HCl (Figure 2b). Further, CO₂ emissions were observed at temperatures of 400–600 °C due to the presence of microcline, albite, calcite, and coal fragments in the initial bentonite along with clay minerals (the measured total C content is about 0.6–0.7%) [24]. Thus, a temperature range above 700 °C was chosen for the synthesis of matrices.

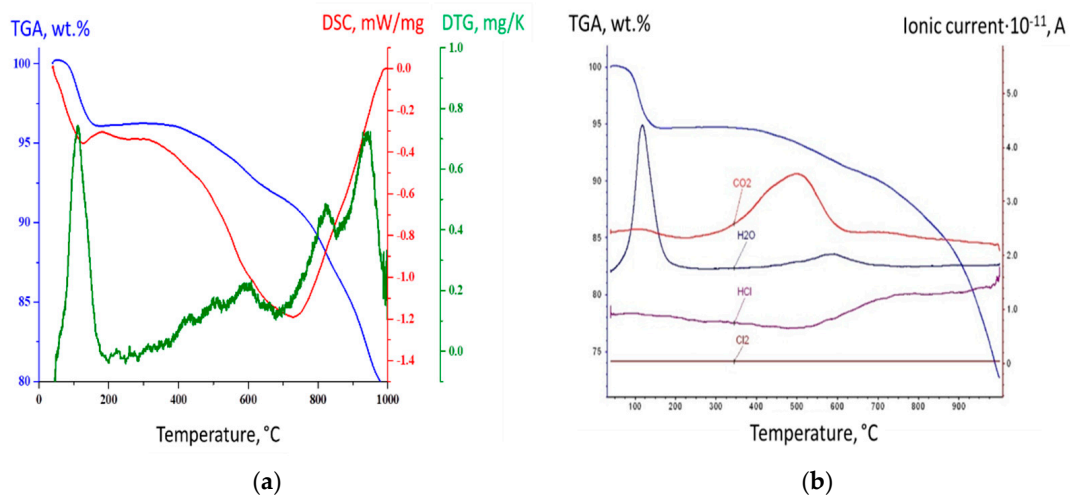


Figure 2. (a) TGA and DSC curves for a sample B20-0; (b) TGA curves together with the composition of the released gases according to mass spectrometry data.

3.2. X-ray Diffraction Analysis

To study phase composition, the synthesized tablets were ground again and sent for XRD analysis; the data were processed using the HighScore Plus program. According to the results, the studied ceramics were polyphase samples with the following main observed phases: leucite KAlSi_2O_6 , albite $\text{K}_{0.2}\text{Na}_{0.8}\text{AlSi}_3\text{O}_8$, sanidine $(\text{Na},\text{K})\text{AlSi}_3\text{O}_8$, spodumene $\text{LiAlSi}_2\text{O}_6$, strontium anorthite $\text{SrAl}_2\text{Si}_2\text{O}_8$, and strontium helenite $\text{Sr}_2\text{Al}_2\text{SiO}_7$. Small quantities of cesium kalsilit CsAlSiO_4 and cesium pollucite $\text{CsAlSi}_2\text{O}_6$ were also observed in some samples.

Figures 3–6 show the XRD patterns for ceramics synthesized without introducing silicon-containing additives, showing the main phases identified in the samples, as well as further possible phases.

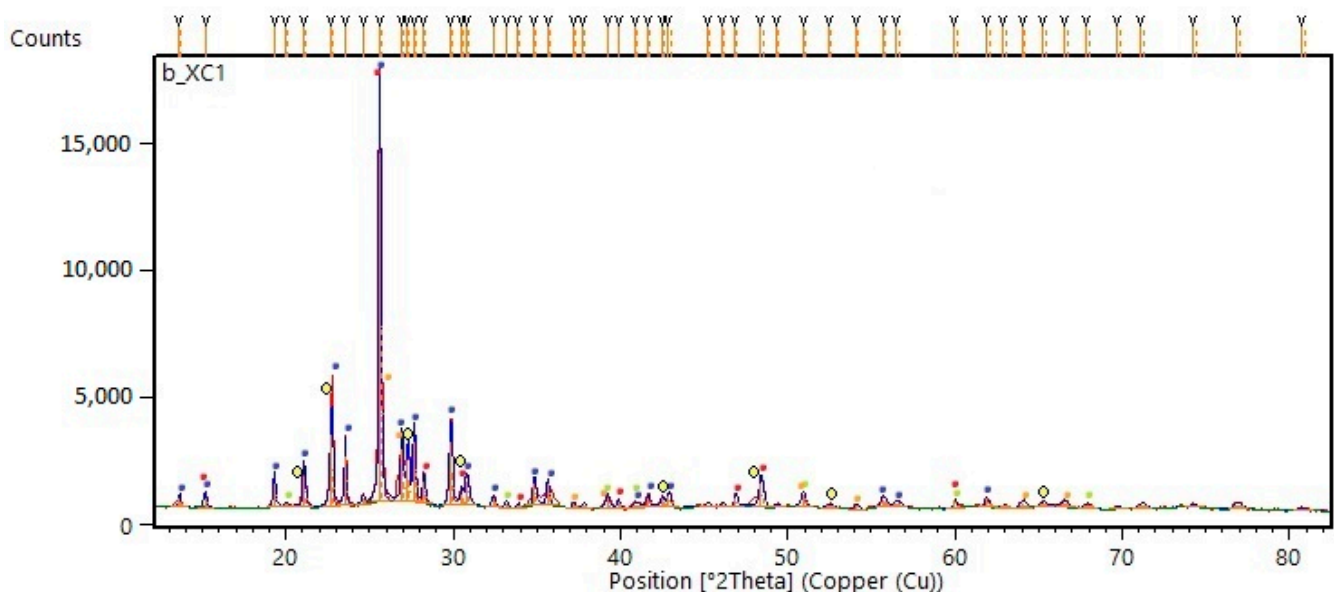


Figure 3. Diffraction pattern of a ceramic sample B20-1; phases: blue— KAlSi_3O_8 , red— $\text{LiAlSi}_2\text{O}_6$, green— $\text{K}_{1.25}\text{Al}_{1.25}\text{Si}_{0.75}\text{O}_4$, yellow— $\text{LiAlSi}_3\text{O}_8$, orange— Al_2SiO_5 .

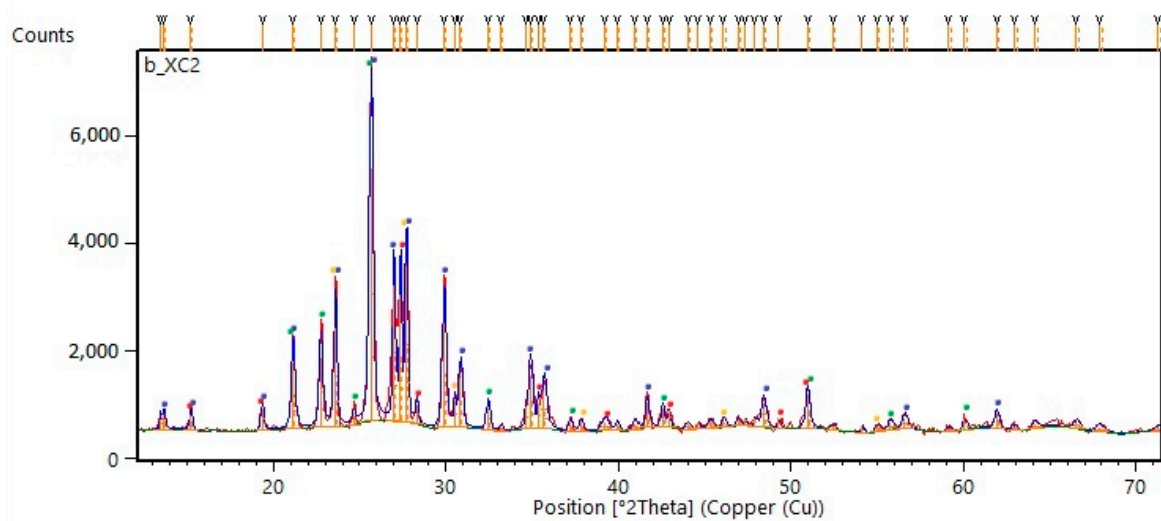


Figure 4. Diffraction pattern of a ceramic sample B20-2; phases: blue— KAlSi_3O_8 , green— $\text{LiAlSi}_3\text{O}_8$, red— $\text{SrAl}_2\text{Si}_2\text{O}_8$, $\text{Sr}_{46}\text{Al}_{92}\text{Si}_{100}\text{O}_{384}$, orange— $\text{CsAlSi}_2\text{O}_6$; Al_2SiO_5 .

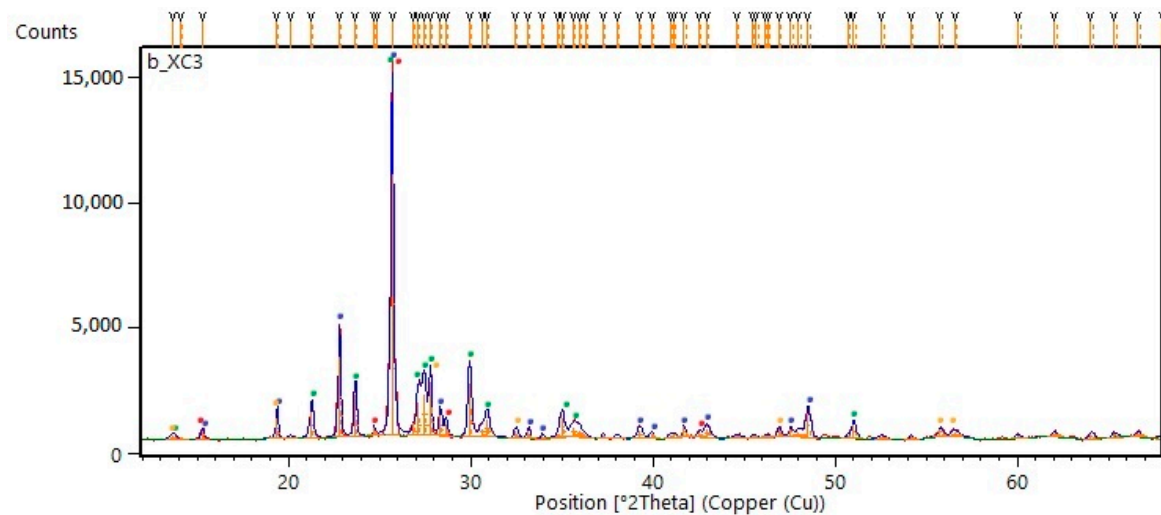


Figure 5. Diffraction pattern of a ceramic sample B20-3; phases: blue— $\text{LiAlSi}_3\text{O}_8$, green— KAlSi_3O_8 , red— KAlSiO_4 , orange— $\text{SrAl}_2\text{Si}_2\text{O}_8$; $\text{K}_{9.71}\text{Al}_{1.68}\text{Si}_{34.32}\text{O}_{72}$.

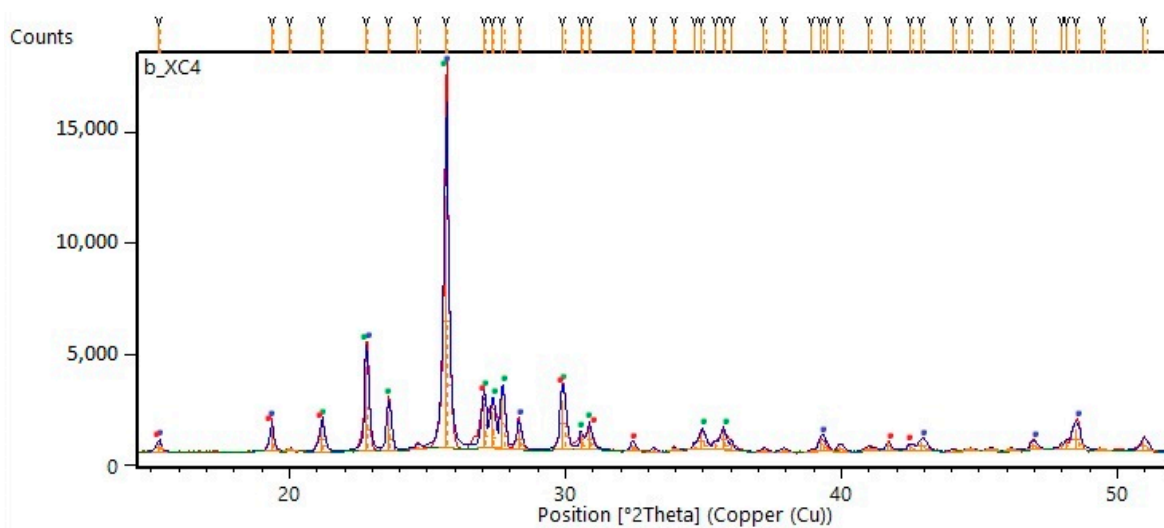


Figure 6. Diffraction pattern of a ceramic sample B20-4; phases: blue— $\text{LiAlSi}_3\text{O}_8$, green— KAlSi_3O_8 , red— $\text{SrAl}_2\text{Si}_2\text{O}_8$.

To better understand the structure transformations that occurred through heating, but not through cooling, an X-ray phase analysis with in situ heating was carried out by heating samples from a temperature of 30 to 1000 °C and then cooling them to 35 °C. Figure 7 shows an example of the combined diffraction patterns for a sample containing 30 wt.% of eutectic. This additional sample was synthesized according to the standard procedure described above and was then investigated in order to reduce the probability of missing phases, because secondary phases with content of less than 5 wt.% could not practically be identified. It should be noted that phase changes already occur at 600 °C, but the most significant structural rearrangements occur at 750 °C. The main crystalline phases occurring at high temperatures are leucite, albite, sanidine, and spodumene, which are framework aluminosilicates capable of retaining cations. The initial phases are not observed in the final products, which means that all cations are incorporated into the new structure.

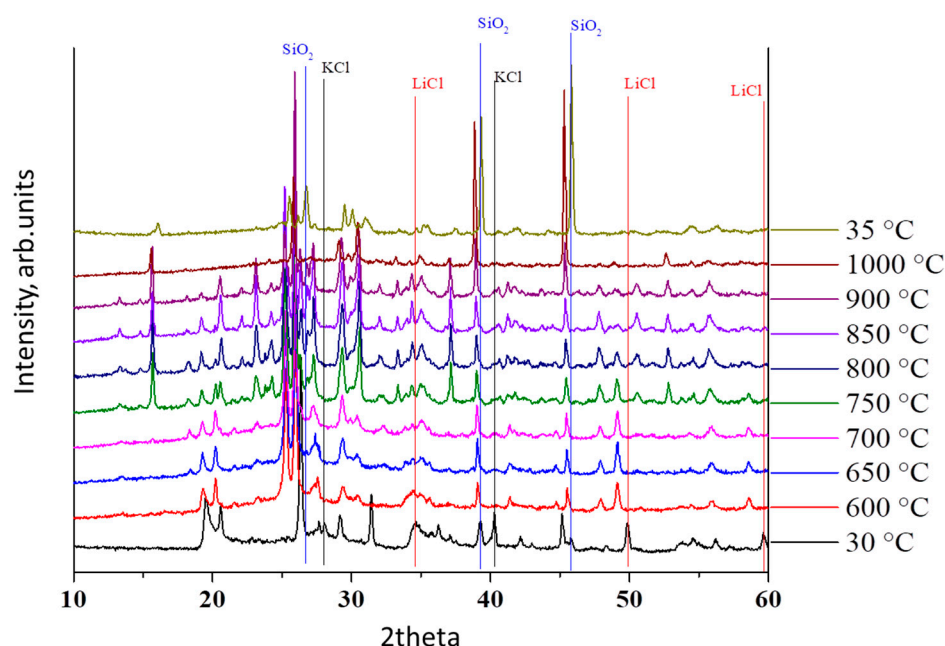


Figure 7. Diffraction patterns of a sample based on bentonite clay with the inclusion of 30 wt.% of simulated spent eutectic LiCl–KCl obtained at different temperatures.

To confirm that cesium and strontium, alongside the main components of the chloride mixture, were incorporated into the structure of aluminosilicates, additional experiments were carried out with an increased amount of chlorides of these metals both in the presence and in the absence of the LiCl–KCl eutectic, with its total amount being 20 wt.%. The XRD results (Figures 8 and 9) show that cesium kalsilit and pollucite, strontium anorthite, and gehlenite (black points, respectively) are formed even in the presence of the eutectic, and thus it can be argued that these metals may be embedded in structures, in small percentages, in the composition of simulated spent electrolyte.

Thus, based on the results of the X-ray phase analysis it can be concluded that, under the chosen synthesis conditions, the incorporation of alkali and alkali earth metals into the structure of aluminosilicates occurs.

A modification of the matrix material made by adding silicon-containing additives did not significantly affect the final major phases in the sample, which can be seen from the XRD results presented in Table 2.

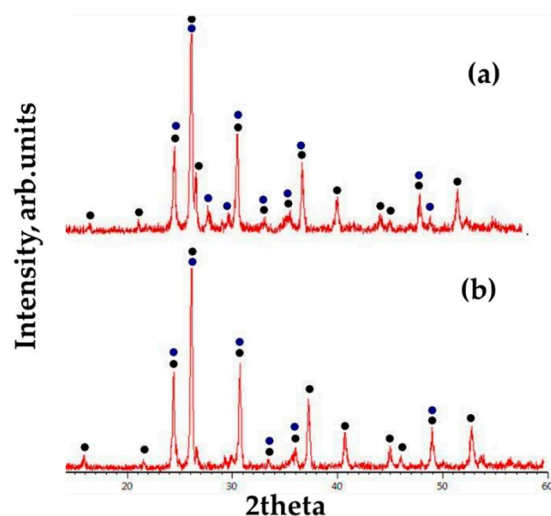


Figure 8. Diffraction patterns of auxiliary samples based on bentonite with an increased content of cesium chloride: black— CsAlSiO_4 , $\text{CsAlSi}_2\text{O}_6$; blue—other phases (KAlSi_3O_8 , $\text{LiAl}(\text{SiO}_3)_2$, $\text{Al}_2(\text{SiO}_4)\text{O}$). (a) 1/4 part of CIM is CsCl , 3/4 parts of CIM—eutectic LiCl-KCl ; (b) 1/2 part of CIM is CsCl , 1/2 part of CIM—eutectic LiCl-KCl .

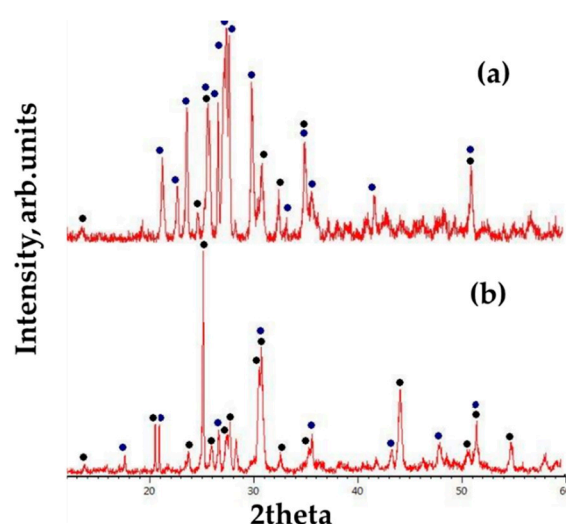


Figure 9. Diffraction patterns of auxiliary samples based on bentonite with an increased content of strontium chloride: black— $\text{SrAl}_2\text{Si}_2\text{O}_8$, $\text{Sr}_2\text{Al}_2\text{SiO}_7$; blue—other phases (KAlSi_3O_8 , $\text{LiAl}(\text{SiO}_3)_2$, $\text{Al}_2(\text{SiO}_4)\text{O}$). (a) 1/4 part of CIM is SrCl_2 , 3/4 parts of CIM—eutectic LiCl-KCl ; (b) 1/2 part of CIM is SrCl_2 , 1/2 part of CIM—eutectic LiCl-KCl .

Table 2. Phase composition of the samples with various silicon-containing additives and including 20 wt.% of the simulated spent eutectic LiCl-KCl .

Nº	Sample Code	Phase Composition
1	B + mcrSi3	$\text{LiAlSi}_3\text{O}_8$, KAlSi_3O_8
2	B + mcrSi5	$\text{LiAlSi}_3\text{O}_8$, KAlSi_3O_8
3	B + mcrSi10	$\text{Li}_2\text{O} \cdot \text{Al}_2\text{O}_3 \cdot 7.5\text{SiO}_2$, KAlSi_3O_8 , $\text{Al}_{2.806}\text{O}_{22.08}\text{Si}_{8.878}$
4	B + NaSi3	$\text{LiAlSi}_3\text{O}_8$, $\text{LiAlSi}_2\text{O}_6$, $\text{K}_{0.831}\text{Na}_{0.169}\text{Al}_1\text{Si}_3\text{O}_8$, KAlSi_3O_8
5	B + NaSi5	$\text{LiAlSi}_2\text{O}_6$, $\text{K}_{0.831}\text{Na}_{0.169}\text{Al}_1\text{Si}_3\text{O}_8$, $\text{K}_{11.7}\text{Al}_{1.8}\text{Si}_{34.2}\text{O}_{72}$
6	B + NaSi10	$\text{LiAlSi}_2\text{O}_6$, $\text{K}_{0.831}\text{Na}_{0.169}\text{Al}_1\text{Si}_3\text{O}_8$, KAlSi_3O_8 , $(\text{Li}_2\text{O} \cdot \text{Al}_2\text{O}_3 \cdot 7.5\text{SiO}_2)$
7	B + A3	KAlSi_3O_8 , $\text{LiAlSi}_3\text{O}_8$
8	B + A5	KAlSi_3O_8 , $\text{LiAlSi}_3\text{O}_8$
9	B + A10	KAlSi_3O_8 , $\text{LiAlSi}_3\text{O}_8$

3.3. Mechanical Compressive Strength

At first the samples with a thickness of 2–4 mm were tested, but were marked as not accurately showing the mechanical properties of the synthesized materials, since such a small measurement did not allow for determining the moment of fracture, due to the rapid transition from fracturing to pressing. Due to this, samples with a greater thickness (8–10 mm) and with masses of ~1 g were prepared. The applied load was up to 5 kN at a speed of 1 mm/min. It was noted that all the tablets disintegrated gradually along the edges while maintaining the main “bulk”. Table 3 shows the results of mechanical tests for some of the most interesting and important samples with regard to the obtained parameters.

Table 3. Test results for mechanical strength.

№	Sample Code	Mechanical Strength, MPa
1	B20-3	60.17
2	B20-4	61.08
3	B + mcrSi3	61.93
4	B + mcrSi10	57.29
5	B + NaSi10	17.77
6	B + A10	55.36

Similar and significantly higher values of mechanical strength are observed for all the samples that had the inclusion of a chloride mixture of various compositions. It should be noted that the addition of even 10 wt.% of microcrystalline silica or AEROSIL did not significantly change this parameter, whereas the addition of the same amount of sodium silicate resulted in the strength decreasing by almost 3 times the amount, but it still exceeded the strength threshold for glass-like materials specified in NP-019-15 (10 MPa).

3.4. Hydrolytic Stability

The results of the hydrolytic stability tests are presented in Table 4.

Table 4. Results of tests to determine hydrolytic stability.

№	Sample Code	Component Leaching Rate on the Last (28th) Day of the Study, g/cm ² ·Day						
		K	Li	Sr	Cs	Al	Si	Cl ⁻
1	B20-1	2.0×10^{-6}	9.4×10^{-6}	-	7.5×10^{-8}	3.3×10^{-8}	5.4×10^{-6}	2.2×10^{-7}
2	B20-2	2.4×10^{-6}	2.7×10^{-5}	1.6×10^{-7}	6.6×10^{-8}	7.6×10^{-8}	2.8×10^{-6}	5.3×10^{-7}
3	B20-3	2.5×10^{-6}	3.7×10^{-5}	4.1×10^{-6}	6.3×10^{-7}	7.1×10^{-8}	3.6×10^{-6}	1.2×10^{-7}
4	B20-4	2.2×10^{-6}	2.3×10^{-5}	8.0×10^{-7}	8.1×10^{-8}	7.4×10^{-8}	3.0×10^{-6}	3.0×10^{-7}
5	B + mcrSi3	3.2×10^{-6}	4.7×10^{-5}	-	-	7.6×10^{-8}	3.1×10^{-6}	2.9×10^{-7}
6	B + mcrSi5	2.7×10^{-6}	2.6×10^{-5}	-	-	9.6×10^{-9}	2.0×10^{-6}	2.7×10^{-7}
7	B + mcrSi10	2.7×10^{-6}	2.0×10^{-5}	-	-	7.8×10^{-9}	1.6×10^{-6}	2.8×10^{-7}
8	B + NaSi3	2.3×10^{-6}	4.4×10^{-5}	-	-	2.4×10^{-7}	3.6×10^{-6}	1.9×10^{-7}
9	B + NaSi5	3.0×10^{-6}	7.7×10^{-5}	-	-	5.9×10^{-7}	8.5×10^{-6}	1.8×10^{-6}
10	B + NaSi10	5.6×10^{-6}	7.7×10^{-5}	-	-	1.1×10^{-7}	7.4×10^{-6}	1.8×10^{-5}
11	B + A3	3.2×10^{-6}	4.8×10^{-5}	-	-	7.5×10^{-8}	8.3×10^{-6}	2.4×10^{-7}
12	B + A5	2.8×10^{-6}	3.6×10^{-5}	-	-	3.2×10^{-8}	5.2×10^{-6}	2.6×10^{-7}
13	B + A10	5.4×10^{-6}	1.6×10^{-4}	-	-	3.9×10^{-7}	2.0×10^{-5}	2.3×10^{-7}

The leaching rate of elements from ceramic samples meets the regulatory requirements for homogeneous forms of HLW (10^{-6} g/cm²·day). It may also be noted that the leaching rate on the 28th day of the main elements of the sample is quite low for all the samples studied, which confirms their chemical stability.

3.5. Effect of Irradiation on the Characteristics of the Samples

Figure 10 presents the data on the mechanical strength of ceramic samples before and after irradiation. The data presented in Figure 10 show that the synthesized samples do not significantly lose their mechanical characteristics for the entire range of doses up to

10^9 Gy. All the samples have a sufficient mechanical strength according to the normative document for homogeneous HLW (>10 MPa).

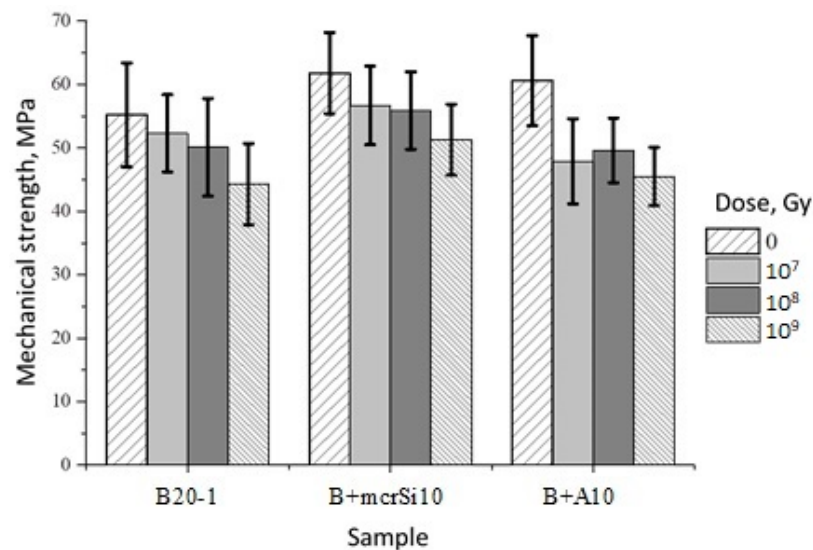


Figure 10. Dependence of the mechanical strength of samples on the dose of ionizing radiation.

Figures 11 and 12 show a comparison of the X-ray diffraction patterns of the samples B20-1 and B + mcrSi10 before and after irradiation with electrons up to a dose of 10^9 Gy. The phase composition remains practically unchanged after high doses of irradiation to ceramic samples. A slight broadening of peaks and a decrease in the intensity of individual peaks are noticeable. The relative content of minor mineral phases changes insignificantly from sample to sample, but this is most likely due to the heterogeneity of the samples.

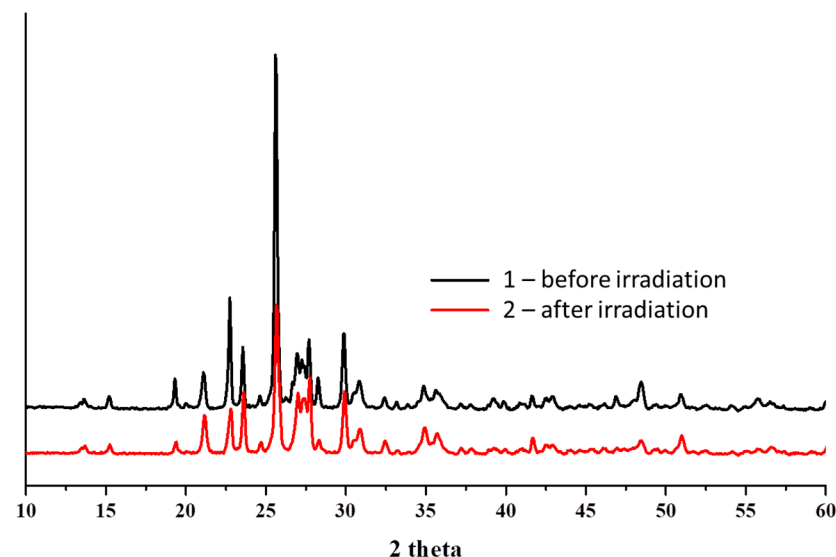


Figure 11. Comparison of the X-ray diffraction patterns of the sample B20-1 before irradiation (1) and after irradiation to the absorbed dose of 10^9 Gy (2).

The scanning electron microscope images indicate that there is practically no difference in surface morphology between the samples before and after irradiation (Figure 13). The samples are characterized by the alternation of large aggregates 5 . . . 50 μm in size. The irradiated samples did not show the appearance of any new formations different from those observed in the original samples, or the development of defects in the form of microcracks and channels.

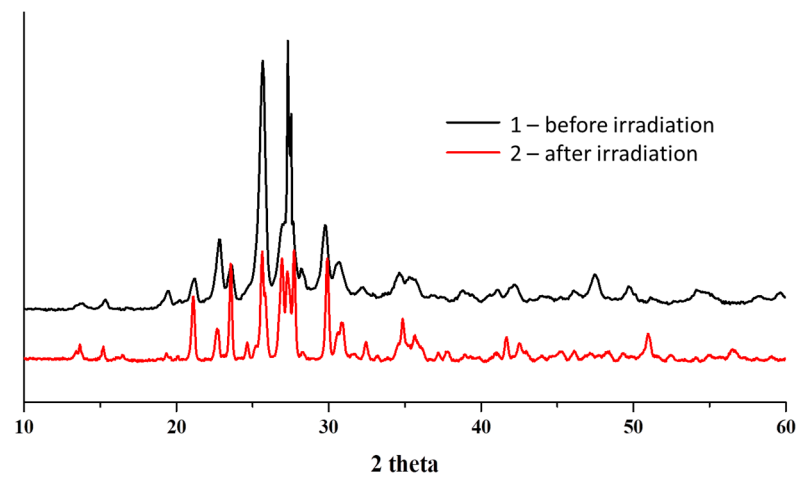


Figure 12. Comparison of the X-ray diffraction patterns of the sample B + mcrSi10 before irradiation (1) and after irradiation to the absorbed dose of 10^9 Gy (2).

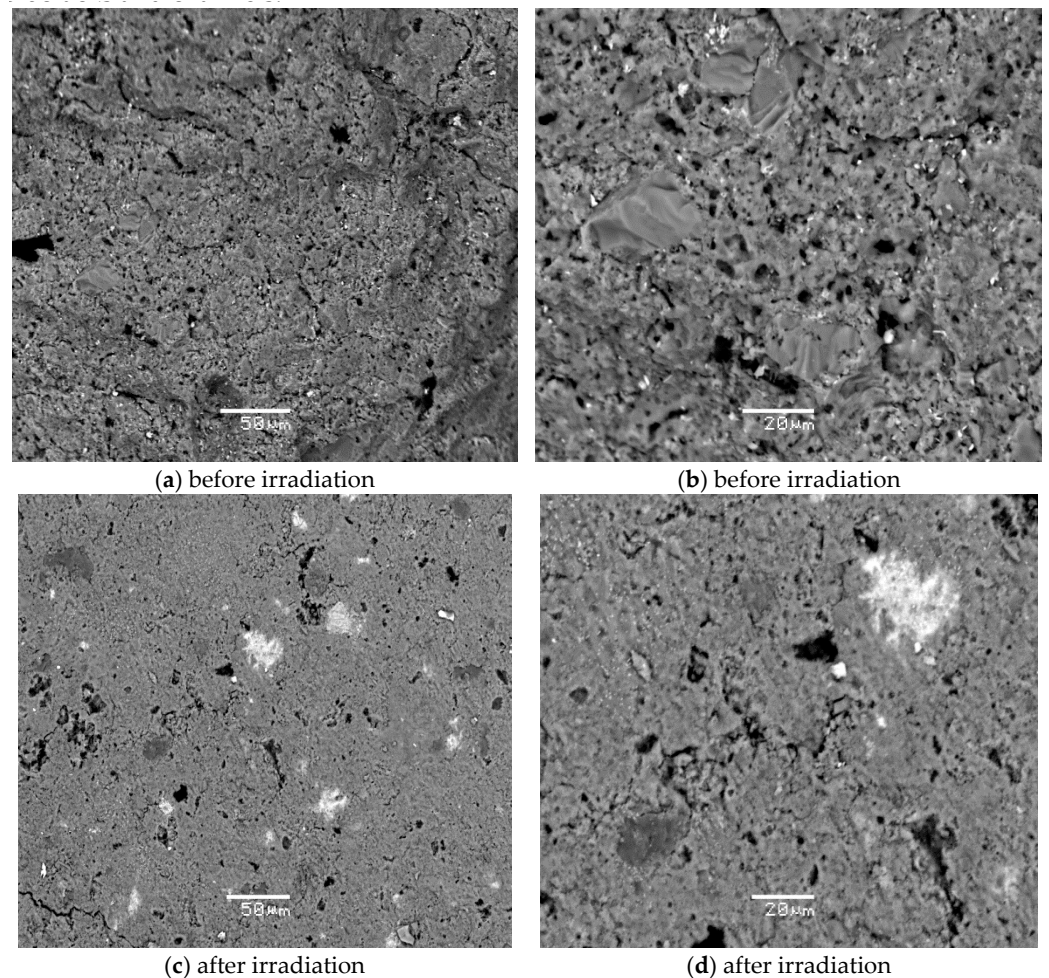


Figure 13. SEM images of the samples with composition B20-1 before and after irradiation by electrons to the absorbed dose of 10^9 Gy.

Figure 13 shows the SEM images of the sample with composition B20-1. Figure 13a,b show that the sample generally has low porosity, and that its composition is uniform, since there are no areas that differ greatly in shade. The shade in these SEM images reflects the average atomic number of an element—the lighter areas correspond to elements with a higher atomic number (for example, cesium). After irradiation (Figure 13c,d), individual

lighter areas corresponding to the level of cesium minerals become more visible. The uneven distribution may be associated with both irradiation and with the initial uneven distribution of individual small crystallites of cesium minerals.

The morphological composition of the samples is diverse and is represented by both individual crystallites and glassy materials with crystallites scattered over the surface. Glass is similar in composition to feldspar (similar to rhyolite, but the K content is greater than Na).

Thus, we can conclude that electron irradiation doses of up to 10^9 Gy do not significantly affect the phase composition and structural characteristics of the studied ceramic samples.

4. Conclusions

We obtained samples of ceramic materials made of bentonite clay, with the addition of the 20 wt.% LiCl–KCl eutectic as a simulator of the spent electrolyte from pyrochemical reprocessing of SNF. The samples' phase composition, mechanical, hydrolytic, and radiation stabilities were studied. The results from this study indicate that the investigated matrix compositions and the method of their synthesis provide the samples with parameters that meet the regulatory requirements for solidified HLW, such as:

- Specific mechanical characteristics (compressive strength ≥ 10 MPa);
- Radiation resistance (without changes in mechanical strength and structure at an absorbed dose of up to 10^9 Gy);
- Leaching rate (for all components $\leq 10^{-6}$ g/(cm²·day)).

Thus, it was confirmed that bentonite clays can be used as a starting material for the immobilization of HLW produced from SNF pyrochemical processing. Such HLW may consist of chlorides of alkali and alkali earth metals. In addition, the matrix may be modified by the addition of silicon-containing additives (microcrystalline silica or AEROSIL). The level of additives present may be between 10 and 20 wt.%. Such additives can help to lower the temperature of matrix synthesis.

Author Contributions: Conceptualization, V.G.P. and A.A.Z.; methodology, V.G.P. and A.P.V.; formal analysis, A.V.M. and I.V.M.; investigation, A.V.M.; resources, V.G.P., S.N.K. and A.A.Z.; writing—original draft preparation, A.V.M.; writing—review and editing, V.G.P. and A.V.G.; visualization, A.V.M. and V.G.P.; supervision, V.G.P.; project administration, A.P.V.; funding acquisition, V.G.P. All authors have read and agreed to the published version of the manuscript.

Funding: A.V.M. was funded by the Russian Foundation for Basic Research, grant number 19-33-90072.

Data Availability Statement: Not applicable.

Conflicts of Interest: The authors declare no conflict of interest.

References

1. Jantzen, C.M. Development of glass matrices for high level radioactive wastes. In *Handbook of Advanced Radioactive Waste Conditioning Technologies*; Ojovan, M.I., Ed.; Woodhead Publishing Limited: Cambridge, UK, 2011; pp. 230–292.
2. Mochalov, Y.S. Report on the Project Direction “Proryv”: “Place and Advantages of the Project in the Development of the World Energy System”, 7–8, June 2016. Available online: <http://proryv2020.ru/en/opinion/> (accessed on 13 September 2021).
3. Sobolev, I.A.; Ozhovan, M.I.; Shcherbatova, T.D.; Batyukhnova, O.G. *Glasses for Radioactive Waste*; Energoatomizdat: Moscow, Russia, 1999.
4. Lee, K.R.; Riley, B.J.; Park, H.S.; Choi, J.H.; Han, S.Y.; Hur, J.M.; Peterson, J.A.; Zhu, Z.; Schreiber, D.K.; Kruska, K.; et al. Investigation of physical and chemical properties for upgraded SAP (SiO₂Al₂O₃P₂O₅) waste form to immobilize radioactive waste salt. *J. Nucl. Mat.* **2019**, *515*, 382–391. [[CrossRef](#)]
5. Lavrinovich, Y.G.; Kormilitsyn, M.V.; Konovalov, V.I.; Tselishchev, I.V.; Tomilin, S.V.; Chistyakov, V.M. Vitrification of chloride wastes in the pyroelectrochemical method of reprocessing irradiated nuclear fuel. *At. Energy* **2003**, *95*, 781–785. [[CrossRef](#)]
6. Leturcq, G.; Grandjean, A.; Rigaud, D.; Perouty, P.; Charlot, A.M. Immobilization of fission products arising from pyrometallurgical reprocessing in chloride media. *J. Nucl. Mat.* **2005**, *347*, 1–11. [[CrossRef](#)]
7. Lutze, W.; Ewing, R.C. *Radioactive Waste Forms for the Future*; Elsevier Science Pub. Co. Inc.: New York, NY, USA, 1988; p. 712.
8. Weber, W.J. Radiation and Thermal Ageing of Nuclear Waste Glass. *Proc. Mat. Sci.* **2014**, *7*, 237–246. [[CrossRef](#)]

9. Stanek, C.R.; Uberuaga, B.P.; Scott, B.L.; Feller, R.K.; Marks, N.A. Accelerated chemical aging of crystalline nuclear waste forms. *Curr. Opin. Solid State Mat. Sci.* **2012**, *16*, 126–133. [CrossRef]
10. Leinekugel-le-Cocq-Errien, A.Y.; Deniard, P.; Jobic, S.; Gautier, E.; Evain, M.; Aubin, V.; Bart, F. Structural characterization of the hollandite host lattice for the confinement of radioactive cesium: Quantification of the amorphous phase taking into account the incommensurate modulated character of the crystallized part. *J. Solid State Chem.* **2007**, *180*, 322–330. [CrossRef]
11. Marra, J.; Billings, A.; Brinkman, K.; Fox, K. Development of Ceramic Waste Forms For An Advanced Nuclear Fuel Cycle (No. SRNL-STI-2010-00622). Savannah River Site 2010. Available online: <https://digital.library.unt.edu/ark:/67531/metadc834515/> (accessed on 13 September 2021).
12. Zaripov, A.R.; Orlova, V.A.; Pet'kov, V.I.; Slyunchev, O.M.; Galuzin, D.D.; Rovnyi, S.I. Synthesis and study of phosphate $\text{Cs}_2\text{Mn}_{0.5}\text{Zr}_{1.5}(\text{PO}_4)_3$. *Russ. J. Inorg. Chem.* **2009**, *54*, 45–51. [CrossRef]
13. Yudinsev, S.V. Complex Oxides of the Structural Types of Pyrochlore, Garnet and Murataite—Matrices for Immobilization of Actinide Waste from Nuclear Power. Ph.D. Thesis, Russian Academy of Sciences, Moscow, Russia, 2009.
14. Kryukova, A.I.; Kulikov, I.A.; Artemyeva, G.Y. Crystalline phosphates of the family $\text{NaZr}(\text{PO}_4)_3$ —Radiation resistance. *Radiochemistry* **1992**, *34*, 194–200.
15. Oota, T.; Yamai, I. Thermal Expansion Behavior of $\text{NaZr}_2(\text{PO}_4)_3$ Type Compounds. *J. Am. Ceram.* **1986**, *69*, 1–6. [CrossRef]
16. Orlova, A.I.; Kemenov, D.V.; Samoilov, S.G.; Kazantsev, G.N.; Pet'kov, V.I. Thermal expansion of NZP-family alkali-metal (Na, K) zirconium phosphates. *Inorg. Mat.* **2000**, *36*, 830–834. [CrossRef]
17. Pet'kov, V.I.; Dorokhova, G.I.; Orlova, A.I. Architecture of phosphates with $\{[\text{L}_2(\text{PO}_4)_3]^{P^-}\}_{3\infty}$ frameworks. *Crystallogr. Rep.* **2000**, *46*, 76–81.
18. Kim, E.; Kim, J.; Kim, J.; Yoo, J.; Lee, J. Method for Preparing Immobilization Product of Waste Chloride Salts Using Zeolite Only. Korea Patent 0089993, 7 September 2007.
19. Koyama, T. Method to Synthesize Dense Crystallized Sodalite Pellet for Immobilizing Halide Salt Radioactive Waste. U.S. Patent 5340506, 23 August 1994.
20. Lewis, M.A.; Pereira, C. Method of Preparing Sodalite from Chloride Salt Occluded Zeolite. U.S. Patent 5613240, 18 March 1997.
21. Babad, H.; Strachan, D.M. Method for Immobilizing Radioactive Iodine. U.S. Patent 4229317, 10 September 1980.
22. Toshiyuki, N.; Kenichi, O.; Shinzo, U. Production Method for Sodalite Type Waste Solid, and its Baking Device. Japan Patent 255083, 2002.
23. Hiroyasu, K.; Toshiyuki, N.; Kenichi, O.; Wataru, S.; Shinzo, U. Synthesizing Method of Sodalite Type Radioactive Waste Solidified Body. Japan Patent 346994, 1996.
24. Belousov, P.E.; Krupskaya, V.V.; Zakusin, S.V.; Zhigarev, V.V. Bentonite clays from 10th khutor deposit: Features of genesis, composition and adsorption properties. *RUDN J. Eng. Res.* **2017**, *18*, 135–143. [CrossRef]